Accepted Manuscript

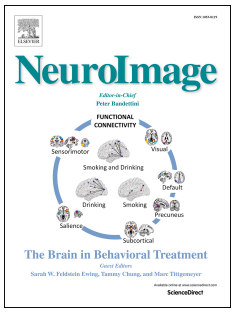

The central autonomic network at rest: Uncovering functional MRI correlates of time-varying autonomic outflow

G. Valenza, R. Sclocco, A. Duggento, L. Passamonti, V. Napadow, R. Barbieri, N. Toschi

PII: S1053-8119(19)30367-2

DOI: https://doi.org/10.1016/j.neuroimage.2019.04.075

Reference: YNIMG 15831

To appear in: *NeuroImage*

Received Date: 30 November 2018

Revised Date: 8 April 2019

Accepted Date: 29 April 2019

Please cite this article as: Valenza, G., Sclocco, R., Duggento, A., Passamonti, L., Napadow, V., Barbieri, R., Toschi, N., The central autonomic network at rest: Uncovering functional MRI correlates of time-varying autonomic outflow, *NeuroImage* (2019), doi: https://doi.org/10.1016/j.neuroimage.2019.04.075.

This is a PDF file of an unedited manuscript that has been accepted for publication. As a service to our customers we are providing this early version of the manuscript. The manuscript will undergo copyediting, typesetting, and review of the resulting proof before it is published in its final form. Please note that during the production process errors may be discovered which could affect the content, and all legal disclaimers that apply to the journal pertain.

ACCEPTED MANUSCRIPT

The central autonomic network at rest: uncovering functional MRI correlates of time-varying autonomic outflow

G Valenza[*](1,2), R Sclocco[*](3,4), A. Duggento (5), L. Passamonti (6), V. Napadow (3), and R Barbieri[#](7) N Toschi[#](3,5)

(1) Bioengineering and Robotics Research Centre “E. Piaggio”, University of Pisa, Pisa, Italy.
(2) Dept. of Information Engineering, University of Pisa, Pisa, Italy.
(3) Athinoula A. Martinos Center for Biomedical Imaging, Department of Radiology, Massachusetts General Hospital, Harvard Medical School, Charlestown, MA, USA
(4) Department of Radiology, Logan University, Chesterfield MOU, USA
(5) Dept. of Biomedicine and Prevention, University of Rome "Tor Vergata", Rome, Italy
(6) Department of Clinical Neurosciences, University of Cambridge, Cambridge, UK.
(7) Dept. of Electronics, Informatics and Bioengineering, Politecnico di Milano, Milano. Italy.

* These authors contributed equally to this work
# These authors contributed equally to this work

Corresponding Author:

Gaetano Valenza, Ph.D.
Department of Information Engineering
Bioengineering and Robotics Research Center "E. Piaggio,"
School of Engineering, University of Pisa
Largo Lucio Lazzarino 1
56122 Pisa, Italy
Email: g.valenza@ieee.org

Running title: Central autonomic network at rest

Keywords: Human Connectome Project, Central Autonomic Network, Point Process, Heart Rate Variability, Autonomic Nervous System

ACCEPTED MANUSCRIPT

Abstract

Peripheral measures of autonomic nervous system (ANS) activity at rest have been extensively employed as putative biomarkers of autonomic cardiac control. However, a comprehensive characterization of the brain-based central autonomic network (CAN) sustaining cardiovascular oscillations at rest is missing, limiting the interpretability of these ANS measures as biomarkers of cardiac control.

We evaluated combined cardiac and fMRI data from 34 healthy subjects from the Human Connectome Project to detect brain areas functionally linked to cardiovagal modulation at rest. Specifically, we combined voxel-wise fMRI analysis with instantaneous heartbeat and spectral estimates obtained from inhomogeneous linear point-process models.

We found exclusively negative associations between cardiac parasympathetic activity at rest and a widespread network including bilateral anterior insulae, right dorsal middle and left posterior insula, right parietal operculum, bilateral medial dorsal and ventrolateral posterior thalamic nuclei, anterior and posterior mid-cingulate cortex, medial frontal gyrus/pre-supplementary motor area. Conversely, we found only positive associations between instantaneous heart rate and brain activity in areas including frontopolar cortex, dorsomedial prefrontal cortex, anterior, middle and posterior cingulate cortices, superior frontal gyrus, and precuneus.

Taken together, our data suggests a much wider involvement of diverse brain areas in the CAN at rest than previously thought, which could reflect a differential (both spatially and directionally) CAN activation according to the underlying task. Our insight into CAN activity at rest also allows the investigation of its impairment in clinical populations in which task-based fMRI is difficult to obtain (e.g., comatose patients or infants).

ACCEPTED MANUSCRIPT

Introduction

The central nervous system and autonomic nervous systems (CNS, ANS, respectively) are tightly and dynamically interconnected throughout anatomical, functional, and hormonal pathways (Allen et al., 2015; Beissner et al., 2013; Benarroch, 1993; Cechetto and Saper, 1990; Sclocco et al., 2016a; Sclocco et al., 2016b; Thayer et al., 2012). The parasympathetic effector system originates in the brainstem and sacral region of the spinal cord, whereas the sympathetic effector system arises in its thoracic and lumbar regions. In the context of controlling heart function, these two autonomic branches also interact at the level of the atrial sinus node to concurrently regulate heart rate (HR) and, consequently, blood pressure and respiration dynamics (Benarroch, 1993; Cechetto and Saper, 1990).

While spectral analysis of heartbeat interval series (i.e., the beat-to-beat HR variations) can provide reliable markers of parasympathetic autonomic outflow through integration in the high frequency band, estimates of purely sympathetic activity cannot be easily derived from heart rate variability (HRV) analysis because of the overlapping activity of the two autonomic branches in the low frequency (LF) band (Reyes del Paso et al., 2013). Furthermore, although HF-HRV quantification provides a well characterized estimate of parasympathetic outflow and has been widely used to assess autonomic function at rest and during cognitive/emotional tasks (Kamath and Fallen, 1993; Lombardi et al., 1996; Malik et al., 1996; Thayer et al., 2012; Thayer and Lane, 2007), the brain correlates of HF-HRV dynamics have not been fully elucidated. Only a few studies have explored the relationship between HF-HRV fluctuations and cortical/subcortical fMRI signal dynamics (Napadow et al., 2008; Chang et al., 2013; Nikolaou et al., 2016; Sclocco et al., 2016a; Sclocco et al., 2016b). This significantly limits the interpretation of such estimates in terms of understanding the neurobiology of the autonomic systems and its related disorders.

The set of brain regions involved in autonomic modulation and control have thus far been referred to as the central autonomic network (CAN) (Benarroch, 1993; Cechetto and Saper, 1990; Saper, 2002; Verberne and Owens, 1998). In addition to the primary role played by the brainstem nuclei (such as the nucleus tractus solitarii (NTS) in the medulla or the parabrachial nucleus (PBN) in the pons), a number of forebrain regions have also been proposed as key components of the CAN, including the cingulate cortex, insula, medial prefrontal cortex, thalamus, amygdala, and hypothalamus (see (Benarroch, 2012) for details). Thus far, many studies employing HRV-neuroimaging measures to explore the functional neuroanatomy of the CAN have been based on manipulating the subject's arousal via somatosensory/motor, cognitive, or affective tasks, while cardiac activity was being recorded through electrocardiogram or photoplethysmography (Matsunaga et al., 2009; Goswami et al., 2011; Nugent et al., 2011). Several studies have also explored heart-brain signal associations at rest, mainly focusing on the fluctuations of dynamic functional connectivity between various regions of interest and HF-HRV

power (Chang et al., 2013) or heart rate (Nikolaou et al., 2016). Still, Over and above the well-known limitations of using task-based functional imaging (i.e., its scarce utility in patients with severe cognitive problems or who are minimally conscious), past studies have also suffered from some methodological issues, especially in the way of computing heartbeat-related spectral estimates with the high temporal resolution (approximately 2 second) (Acharya et al., 2007) needed to match the timescales of functional MRI (fMRI) acquisitions. More specifically, previous analytical pipelines have relied on averaging spectral indices within the duration of the task conditions. However, aside from the loss of time-related effects, by design this approach incorporates task-related polarizations in the recruitment of the CAN, which can possibly result in selective over- or under-representations of the underlying brain regions.

For example, Matsunaga et al. (Matsunaga et al., 2009) found a positive association between the insular cortex response to positive emotions and HF-HRV. A combination of sensory stimulations and motor tasks was also used to explore the representation of somatosensory afferent input within the CAN, suggesting a role of the ventromedial prefrontal cortex and subgenual cingulate cortex in parasympathetic regulation (Goswami et al., 2011). Moreover, Nugent and co-authors found differential correlation patterns between HRV indices and the orbitofrontal cortex metabolism in patients with major depression relative to controls (Nugent et al., 2011). Other studies employed time-frequency decomposition techniques (e.g., wavelets) to estimate continuous HRV frequency components which can then be used as regressors of interest in voxel-wise analyses of fMRI data (Rubio et al., 2015). However, such data-driven approaches do not intrinsically account for the generative mechanisms of cardiovascular dynamics.

The main aim of this study is therefore a deeper characterization of the cortical and subcortical constituents of the CAN in the absence of possible task-related confounds and/or polarizations. Investigating the CAN in task-free conditions is also attractive from a clinical perspective as it may inform and be further implemented in clinical studies in which patient compliance can be problematic (minimally conscious patients, patients with dementia, infants).

We explore the neuronal correlates of cardiovagal control in a task-free experimental setting by exploiting the high data volume per subject and high spatio-temporal resolution of the imaging data provided by the Human Connectome Project (HCP) (McNab et al., 2013). We relate task-free CAN activity to quantitative measures of cardiovagal control via inhomogeneous point-process models of heartbeat dynamics (Barbieri et al., 2005), which allow instantaneous estimation of spectral HRV indices at rest. The ability to obtain HRV measures at any time resolution is critical to match their temporal dynamics to those of the fMRI data. Of note, our analytical framework does not require any pre-processing stages (e.g., interpolation) (Barbieri et al., 2005; Napadow et al., 2008), and has been successfully applied to specific tasks that evaluate

the modulation of CAN activity during hand grip (Napadow et al., 2008), visually-evoked motion sickness (Sclocco et al., 2016b), continuous pain (Sclocco et al., 2016a).

Combined with the HRV estimation method that we have recently developed, the HCP dataset represents the ideal candidate for studying the neural correlates of the autonomic outflow in a task-free condition. Although this was an exploratory study, on the basis of our preliminary results (Valenza et al., 2017), as well as of previous literature (as reviewed by Beissner et al., 2013), we also hypothesized that the functional neuroanatomy of the CAN would be more widespread and diffuse than originally described by Benarroch (1993).

Methods

Dataset

The individual datasets used in this study are selected among those included in the "100-unrelated subjects" data release from the Human Connectome Project (HCP U100, 1200 data release). The dataset consists of young, healthy adults (age range: 22-36 years) and exclusion criteria include any medical or neuro-psychiatric disorder, such as hypertension, alcohol abuse, anxiety or depressive disorders. Demographics data are shown in **Table I**, and details about subject selection are presented as **Supplementary Materials**.

Age (years)	**28.82 ± 3.37**
Education (years)	15.03 ± 1.73
Height (inches)	66.97 ± 3.22
Weight (pounds)	172.03 ± 39.92
Body mass index	26.76 ± 4.61
Systolic blood pressure (mmHg)	127.38 ± 13.86
Diastolic blood pressure (mmHg)	79.35 ± 9.14
Cigarettes per week (Number)	7.21 ± 21.20
Drinks per week (Number)	4.47 ± 5.00
Right-Handedness (%)	62.35 ± 54.73
Ethnicity (%)	85.29% white; 5.88% Unknown or Not Reported; 5.88% Black or African American; 2.94% More than one
Race (%)	79.41% Not Hispanic/Latino; 20.59% Hispanic/Latino
Female (%)	52.94%

Table I – *Demographics for the sample population included in the study.*

MRI and physiological data acquisition

Detailed scanning and analysis procedures are available on the HCP release manual (www.humanconnectome.org), and an overview of the workflow of the present study is shown in **Figure 1**. Briefly, participants were scanned on a customized Siemens 3T "Connectome Skyra" scanner at Washington University in St. Louis. For each participant, resting state fMRI (rs-fMRI) data were acquired in separate sessions on two different days, with two runs per day. Subjects were instructed to keep their eyes open and fixed on a bright cross-hair projected on a dark background, presented in a darkened room. Within each session, oblique axial acquisitions alternated between phase encoding in a right-to-left (RL) direction in one run and in a left-to-right (LR) direction in the other run. Gradient-echo echo-planar images (EPI) were collected with the following parameters: TR = 720 ms, TE = 33.1 ms, flip angle = 52 deg, FOV = 208 x 180 mm, matrix = 104 x 90, 72 slices, 2.0 mm isotropic voxel size, multiband factor = 8, echo spacing = 0.58 ms, BW = 2290 Hz/Px. For each run, 1200 volumes were collected, for a total duration of approximately 15 minutes. During the first MRI session, a T1-weighted structural volume (3D MPRAGE, TR = 2400 ms, TE = 2.14 ms, TI = 1000 ms, flip angle = 8 deg, FOV = 224 x 224 mm, 0.7 mm isotropic voxel size, BW = 210 Hz/Px, multiband factor = 2), as well as spin echo field maps using both RL and LR phase encoding, were collected to aid preprocessing and registration of the functional data.

Concurrently with fMRI images, cardiac and respiratory signals were collected using a standard Siemens pulse oximeter placed on a digit and a respiratory belt placed on the abdomen, with a sampling rate of 400 Hz. Since a good quality (and availability) of the finger pulse recordings is instrumental for the correct estimation of HRV indices, cardiac data from each subject were manually and carefully evaluated by an expert observer (RB) in terms of signal-to-noise ratio (SNR), presence of ectopic beats, missing data, or other noticeable artifacts that would affect the HRV analysis. Given the paucity (see below) of subject in which all 4 sessions had acceptable signal quality, and in order to avoid inter-session bias, we chose to include only subjects in which both datasets from the same session were usable, and therefore included exactly one session (i.e. two acquisitions of 1200 volumes each) per subject. This resulted in a final dataset including 34 complete subjects with exactly two usable runs performed on the same day. Individual quality assessments of cardiac recordings, as well as the final list of subjects, are detailed in the **Supplementary Materials**.

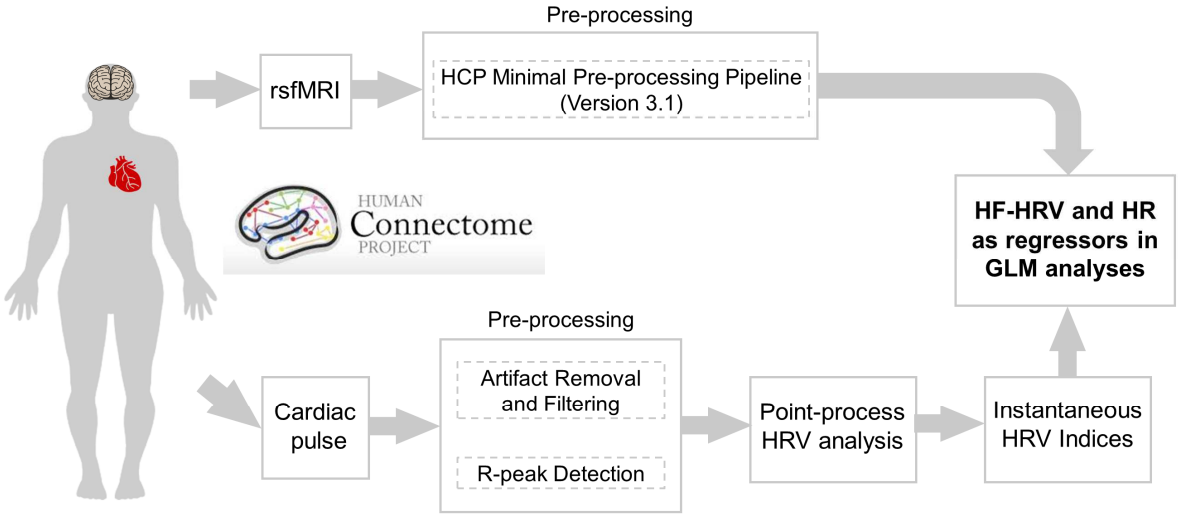

Figure 1 – *Overview of the HRV / fMRI analysis workflow.*

fMRI data preprocessing

rs-fMRI runs were preprocessed by the HCP consortium according to Version 3.1 of the HCP minimal preprocessing pipeline (detailed in (Glasser et al., 2013)) using the Oxford Centre for Functional MRI of the Brain (FMRIB) Software Library (FSL), see https://www.humanconnectome.org/storage/app/media/documentation/s1200/HCP_S1200_Release_Reference_Manual.pdf for details. Specifically, it included gradient distortion correction, motion correction (FSL FLIRT) using a reference volume (SBRef) as target, and susceptibility-induced distortion correction (FSL TOPUP). The transformation of the functional data to a standard MNI space involved several steps: first, the reference volume SBRef was distortion-corrected and registered to the structural T1 image using a customized 2-step Boundary-Based Registration procedure (BBR). The T1-weighted volume was then nonlinearly transformed to MNI space. Finally, all the transformations were applied to the individual EPI volumes, that were also intensity-normalized, corrected for bias field, and brain masked. rs-fMRI data were then denoised using a combination of Independent Component Analysis (FSL MELODIC) followed by an automated component classifier (FMRIB's ICA-based X-noisifier, FIX) that removes movement artifacts as well as other noise source such as physiological noise (Griffanti et al., 2014; Salimi-Khorshidi et al., 2014; Smith et al., 2013). Minimal spatial smoothing (FWHM = 4 mm) was applied. Note that the choice of a smoothing kernel with FWHM that approximates the characteristic dimension of a voxel was made in order to (possibly) discern autonomic nuclei in the brainstem.

Point-process modeling of heartbeat dynamics

A series of beat-to-beat wave peak intervals (RR) was extracted from the finger pulse signal using in-house beat detection and correction algorithm. The RR series was then modeled using an inverse Gaussian probability function which characterizes the waiting time for the next heartbeat event:

$$f(t|\mathcal{H}_t,\xi(t)) = \sqrt{\frac{\xi_0(t)}{2\pi(t-u_j)^3}}\exp\left\{-\frac{1}{2}\frac{\xi_0(t)[t-u_j-\mu_{\mathrm{RR}}(t,\mathcal{H}_t,\xi(t))]^2}{\mu_{\mathrm{RR}}(t,\mathcal{H}_t,\xi(t))^2(t-u_j)}\right\} \quad (1)$$

where $t \in (0,T]$ is the observation interval, $0 \le u_1 < \cdots < u_k < u_{k+1} < \cdots < u_K \le T$ the times of the events,$\mathrm{RR}_j = u_j u_{j-1} > 0$ the j^{th} RR interval,$\{u_j\}_{j=1}^{J}$ the R-wave events, and $j = \widetilde{N}(t)$ the index of the previous R-wave event before time t,$N(t) = \max\{k: u_k \le t\}$ the sample path of the counting process of the RR interval series, $\widetilde{N}(t) = N(t^-) = \lim_{\tau \to t^-} N(\tau) = \max\{k: u_k < t\}$, $\mathcal{H}_t = (u_j, \mathrm{RR}_j, \mathrm{RR}_{j-1}, \ldots, \mathrm{RR}_{j-M+1})$; $\xi(t)$ the vector of the model time-varying parameters, and$\xi_0(t) > 0$ the shape parameter of the inverse Gaussian distribution. The first order moment of this function, i.e., the mean of the probability function $\mu_{\mathrm{RR}}(t,\mathcal{H}_t,\xi(t))$, is parameterized through a linear autoregressive model of order 8 as a function of the previous RR intervals (Barbieri et al. 2005). A preliminary goodness-of-fit analysis of the data considered in this study confirmed the validity of the entire previously defined range for a time-varying local observation interval of duration W between 60s and 90s (Valenza et al. 2014), and pointed at a reasonable trade-off value of 70s, with a 5ms time resolution. Given local observations within a sliding observation W, it is possible to estimate the unknown time-varying parameter vector that maximizes the local log-likelihood through the well-known Newton-Raphson procedure. The model and all its parameters are recursively updated at each iteration. While the validation of spectral analysis through point-process modeling is beyond the scope of the study, it is important to note that the point-process approach for analysis of heartbeat dynamics has been evaluated and validated in multiple biosignal processing studies, including also (but not only) brain correlates of autonomic activity using fMRI (Barbieri et al. 2005; Duggento et al 2016; Napadow et al. 2008; Sclocco et al. 2016a, 2016b; Valenza et al. 2013, 2017, 2018).

HRV/fMRI analysis

Possible differences across sessions in median heart rate or median HF-HRV power were investigated using the Wilcoxon non-parametric test for paired data. Exemplary instantaneous estimates of the high-frequency components of HRV (HF-HRV), as well as instantaneous heart rate (HR) are shown in **Figure 2**. All series were resampled at the fMRI TR, thresholded at the

98% percentile in order to retain the full dynamics of the HRV signals and increase robustness to outliers, and convolved with a double gamma hemodynamic response function (HRF), in order to be used as regressors of interest in successive joint HRV-fMRI analyses. Statistical parametric mapping was carried out using the FMRI Expert Analysis Tool (FEAT v. 5.90, FSL). At the first level, both positive and negative contrasts were generated for each regressor. A second level fixed effects analysis was used to summarize the within-subject effects (across the two same-day sessions), and the resulting individual parameter estimates, together with their variances, were passed up to a third (group) level, mixed effects analysis (FLAME, FEAT, FSL). The resulting statistical maps were generated using a cluster-forming threshold of $Z > 2.3$ and a corrected cluster-wise significance threshold of $p < 0.05$.

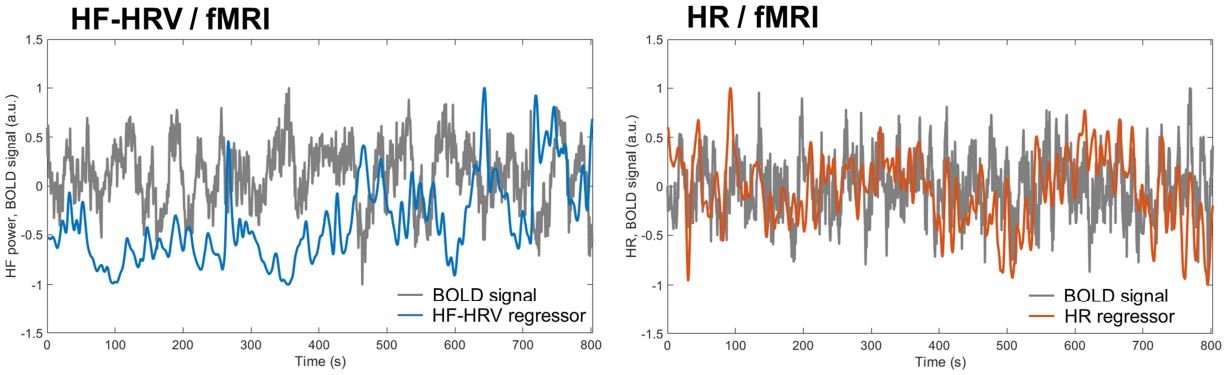

Figure 2 – *Example of instantaneous HF-HRV (left) and HR (right) regressors synchronized with corresponding BOLD signals. Measures in the Y-axis are expressed as arbitrary units (a.u.)*

Results

No statistically significant differences across sessions were found in median heart rate ($p=0.13$, Wilcoxon non-parametric test for paired data) or median HF-HRV power ($p=0.95$, Wilcoxon non-parametric test for paired data). Results from joint HF-HRV fMRI, and HR fMRI analyses are shown in **Figure 3**, and statistically significant clusters ($p < 0.05$, cluster-wise corrected for multiple comparisons) at group level are listed along with their coordinates and localization in **Tables II** and **III**. In the HF-HRV fMRI analysis, all statistically significant clusters revealed a negative relationship between estimated parasympathetic outflow and the BOLD signal. No statistically significant results were found in the opposite contrast. A widespread network of cortical and subcortical regions was involved, including bilateral anterior insulae (aIns), right dorsal middle (dmIns) and left posterior insula (pIns), right parietal operculum (POp), bilateral medial dorsal (MDTh) and ventrolateral posterior thalamic nuclei (VLPTh), anterior mid-cingulate cortex (aMCC), and posterior MCC/medial frontal gyrus/pre-supplementary motor area

ACCEPTED MANUSCRIPT

(pMCC/mFG/pSMA). Other regions showing the same patterns were the primary motor cortex (M1), superior temporal gyrus (STG), right paracentral lobule (PCL), primary visual cortex (V1), fusiform gyrus (FuG), lateral occipital gyrus (lOcG), as well as cerebellar lobule VIIIA (Cereb(VIIIA)).

Conversely, only positive, statistically significant associations were found in the HR-fMRI analysis, with no statistically significant negative association results. For positive associations, significant clusters included left frontopolar cortex (FPC) and left dorsomedial prefrontal cortex (dmPFC), right anterior, posterior, and left posterior/middle cingulate cortices (ACC, MCC, P/MCC), right superior frontal gyrus (SFG), and right precuneus (PCun). Additional clusters encompassed the right angular gyrus (AnG), left superior parietal lobule (SPL), right primary visual cortex (V1), and the left cerebellar lobule V (Cereb(V)) and right cerebellar crus I (Cereb(CrI)).

ACCEPTED MANUSCRIPT

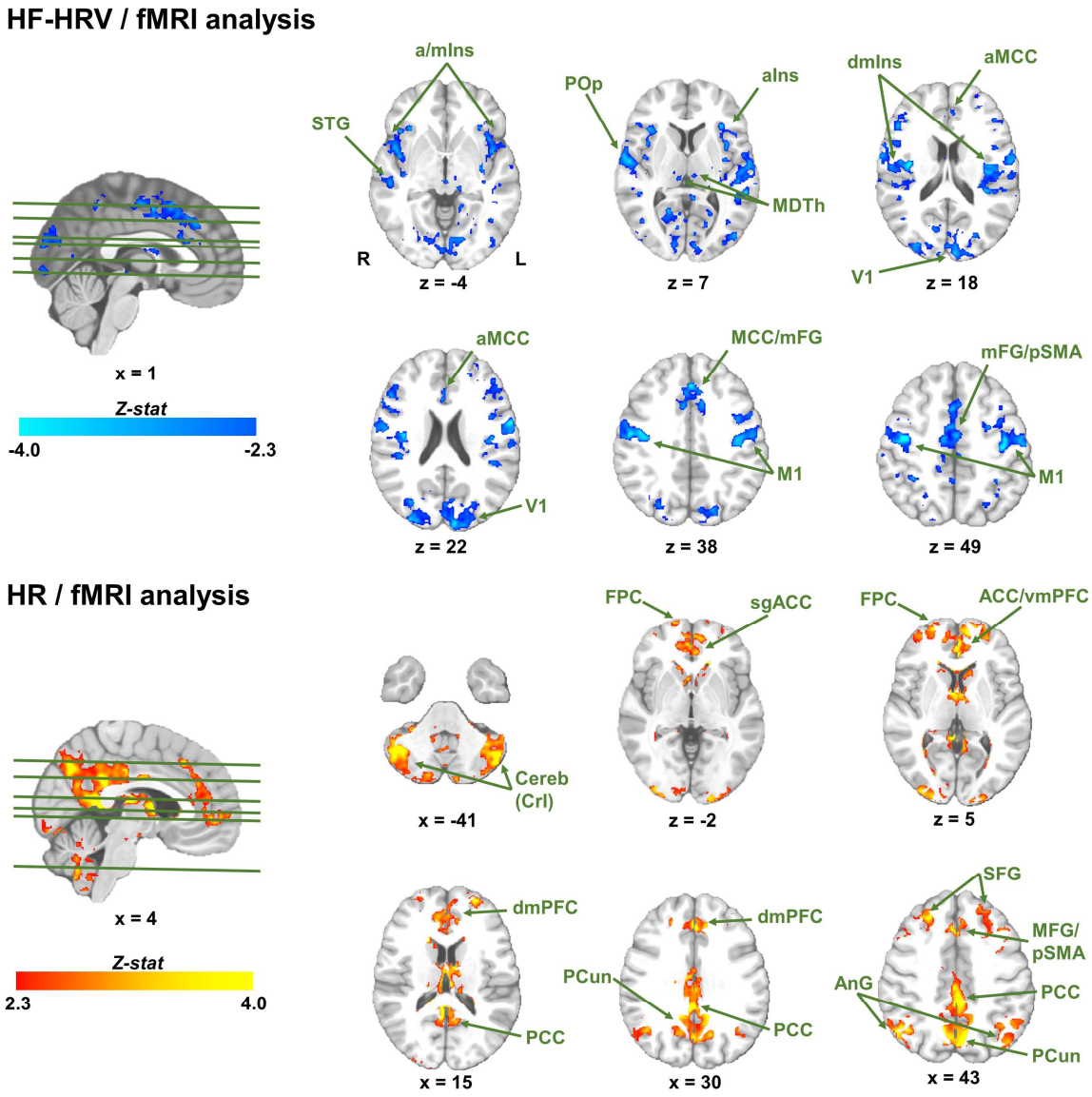

Figure 3 – *Group maps showing the results of the joint HF-HRV/fMRI analysis (top, shades of blue color map) and of the joint HR/fMRI analysis (bottom, red-yellow color map).*

MNI coordinates (mm)			Max z-score	Hemisphere	Region	Label
x	***y***	***z***				
-32	26	2	-4.42	L	Anterior Insula	aIns
38	22	6	-4.02	R	-	-
38	-10	20	-4.47	R	Dorsal Middle Insula	dmIns
-34	-24	12	-4.09	L	Posterior Insula	pIns

2	24	20	-3.48	R	Anterior Middle Cingulate Cortex	aMCC
6	-4	44	-3.91	R	Posterior Middle Cingulate Cortex	pMCC
-8	22	34	-3.49	L	-	-
60	-6	10	-4.49	R	Parietal Operculum	POp
-12	-18	2	-3.54	L	Ventrolateral Posterior Thalamic Nucleus	VLPTh
12	-20	0	-3.34	R	Ventroposterior Lateral Thalamic Nucleus	VPLTh
6	-24	6	-3.07	R	Medial Dorsal Thalamic Nucleus	MDTh
-6	-22	6	-3.09	L	-	-
40	-78	-14	-3.65	R	Lateral Occipital Gyrus	lOcG
-36	-80	-12	-3.48	L	-	-
24	-70	-12	-3.48	R	Fusiform Gyrus	FuG
-22	-70	-8	-3.9	L	-	-
54	-24	-2	-4.23	R	Superior Temporal Gyrus	STG
6	-38	56	-4.12	R	Paracentral Lobule	PCL
-6	4	62	-4.28	L	Superior Frontal Gyrus	SFG
38	-14	44	-4.84	R	Primary Motor Cortex	M1
-40	-20	48	-4.06	L	-	-
18	-56	6	-3.75	R	Primary Visual Cortex	V1
-22	-58	4	-3.22	L	-	-
-20	-64	-46	-3.95	L	Cerebellum Lobule VIIIA	Cereb(VIIIA)

Table II – Localization of significant clusters ($p<0.05$) found in joint HF-HRV/fMRI analysis

MNI coordinates (mm)			**Max z-score**	**Hemisphere**	**Region**	**Label**
x	***y***	***z***				
2	42	6	4.63	R	Anterior Cingulate Cortex	ACC
0	36	26	5.25	-	Posterior ACC	pACC
-2	-36	38	5.45	L	Posterior/Middle CC	P/MCC
4	-44	12	5.34	R	Posterior Cingulate Cortex	PCC
-28	58	12	4.38	L	Dorso-Medial Prefrontal Cortex	dmPFC
-10	58	6	4.55	L	Fronto-Polar Cortex	FPC
2	22	42	4.99	R	Superior Frontal Gyrus	SFG
10	-64	34	5.16	R	PreCuneus	PCun
48	-62	42	4.29	R	Angular Gyrus	AnG

-36	-62	48	3.73	L	-	-
-6	-72	42	5.10	L	Superior Parietal Lobule	SPL
30	-92	-10	4.12	R	Primary Visual Cortex	V1
-20	-96	-8	4.12	L	-	-
-2	-62	-20	4.5	L	Cerebellum Lobule V	Cereb(V)
46	-64	-42	4.81	R	Cerebellum Crus I	Cereb(CrI)
-48	-64	-42	4.71	L	-	-

Table III – Localization of significant clusters ($p<0.05$) found in joint HR/fMRI analysis

Discussion

In this study, the instantaneous estimation of heartbeat dynamics by our point-process approach was paired with brain resting-state fMRI data to characterize the neural correlates of parasympathetic outflow and heart rate in a cohort of 34 young healthy individuals in a task-free experimental setting. Subjects were scanned twice on the same day (total: 2400 volumes per subject) and data were publicly released as part of the HCP dataset. We posit that combining our instantaneous estimation of heartbeat dynamics with the high spatio-temporal resolution and signal-to-noise ratio (SNR) afforded by the HCP dataset allows a robust characterization of the functional neuroanatomy of the CAN at rest.

Group maps from the two analyses revealed widespread and only minimally overlapping networks, showing negative associations between BOLD signals and HF-HRV and positive associations between BOLD signals and instantaneous HR. These results are not directly interpretable in terms of activation/deactivation of brain regions (only a pioneering study in a small cohort exists for such estimates (Duggento et al., 2016)) but can only be conceptualized a temporally synchronous relationship between time series. Nevertheless, our results strongly corroborate previous findings showing that instantaneous HF-HRV is negatively associated to brain responses during nausea (Sclocco et al., 2016b), brainstem function at rest (Sclocco et al., 2016a), or regional perfusion (Allen et al., 2015).

Taken together, our findings (**Figure 3**) confirm and support the key role of the insula, cingulate, frontal/prefrontal cortices, as well as thalamus in the regulation of autonomic outflow demonstrated in previous studies (Beissner et al., 2013; Benarroch, 1993; Cechetto and Saper, 1990; Thayer et al., 2012). Furthermore, our study identified additional regions that were not included in earlier descriptions of the CAN (i.e., as originally described by Benarroch (1993)), but may constitute an important part of its function. These regions include the precuneus, angular gyrus, and cerebellum, which interestingly had been reported in a previous meta-analysis of neuroimaging studies investigating the CAN (Beissner et al., 2013)). However, in addition to these regions, other structures less likely to be involved in autonomic control (such as primary visual cortex and primary motor cortex) have been evidenced by our results. This unexpected

finding may be related to the data-driven, exploratory nature of our study, where no regions or networks of interest were defined a priori. Nevertheless, previous studies combining fMRI and autonomic indices studies reported similar associations, which were particularly consistent in the visual areas (Chang et al., 2013; Nikolaou et al., 2016; Sclocco et al., 2016b). For example, Nikolaou and co-authors found significant correlations between HR and dynamic connectivity values within the visual and somatosensory resting-state networks (Nikolaou et al., 2016).

Unexpectedly, we found no significant association between the two cardiovascular measures and resting-state activity in the amygdala, which is often reported as a core sub-cortical region for emotional processing - especially in response to aversive stimuli (Critchley et al., 2011; LeDoux, 1992)(LeDoux, 2007). Although several possibilities might explain this null finding, we believe that the absence of an effect in the amygdala in this study can be a result of the experimental setting employed, i.e. the fact that subjects were scanned in a resting state condition. In fact, most previous findings reporting associations between amygdala activity and measures of HR variability, have been derived from task-based experiments, during which the autonomic response can be modulated by cognitive, affective, and somatosensory-motor stimuli. In other words, it may be difficult to detect the involvement of the amygdala in autonomic regulation during stress-free, resting conditions.

As expected from previous studies, we also found that the BOLD signal in bilateral anterior, right middle, and left posterior insular cortices was significantly related to instantaneous HF-HRV power (**Figure 3, Table II**). The negative association between the insula fMRI signal at rest and HF-HRV identified here is in keeping with our previous findings showing that greater autonomic response is related to reduced insula response during visually-induced motion sickness (Sclocco et al. 2016b). Likewise, another study assessing the regional cerebral blood flow at rest via arterial spin labelling reported a similar negative correlation between resting HF-HRV and perfusion in frontal operculum (Allen et al. 2015). Together, these results suggest an inhibitory role of the insula over premotor brain stem nuclei that control cardiovagal autonomic outflow (Sclocco et al., 2016a). The insula plays a primary role in aggregating nociceptive and viscero-sensory inputs and play a key role in controlling both sympathetic and parasympathetic activity through descending influence mediated via hypothalamic and brainstem pathways (Benarroch, 2012; Critchley, 2005; Oppenheimer and Cechetto, 2016). The insula is a cytoarchitecturally heterogeneous and complex structure, with the anterior, middle and posterior portions showing differential structural (Mesulam and Mufson, 1982) and functional connectivity properties and patterns (Kurth et al., 2010; Sporns, 2014). The role of the insula in controlling HRV has been supported by studies in patients with different types of stroke or brain tumors (Colivicchi et al., 2004; de Morree et al., 2016) as well as by functional neuroimaging research that has specifically linked insula activity with parasympathetic outflow (Allen et al., 2015; Gianaros et al., 2004). Together with other brain regions, insular grey-matter volume also negatively correlated with HF-HRV in n=185 of healthy individuals, regardless of potentially confounding age and sex differences (Wei et al., 2018).

We also found widespread effects in the cingulate cortex (CC), although with a differential spatial distribution. Specifically, while its middle portion (MCC) was found to be related to cardiovagal fluctuations, the heart rate variations were associated with the cingulate BOLD signal mainly in two broad clusters, one located in the posterior cingulate cortex (PCC) and the other one mainly centered in the pregenual ACC (pgACC). Like the insular cortex, the CC is anatomically heterogeneous, both in terms of its function and of its connectivity patterns (Vogt et al., 1992). An extensive body of work, expertly reviewed in landmark papers (Bush et al., 2000; Devinsky et al., 1995), supports the view of functional specialization of the rostral cingulate in the CAN. More recent studies, however, have suggested that the MCC, previously implicated in cognition, is also important to regulate autonomic activity (Luu and Posner, 2003; Medford and Critchley, 2010), as well as emotional production and perception (Etkin et al., 2011; Kober et al., 2008). Alongside cognitive control (Nee et al., 2007), the anterior portion of the MCC, aMCC, has also been consistently associated to negative affect (Mechias et al., 2010), and pain (Farrell et al., 2005), which suggests a key integrative role of this regions across different psychological domains (Shackman et al., 2011). Finally, ACC/MCC activity has been found to covary with the low-frequency component of HRV during isometric exercise and mental arithmetic (Critchley et al., 2003), or to predict the heart rate response during processing of facial expressions (Critchley, 2005).

Another useful perspective for the interpretation of our results comes from the literature regarding large-scale brain networks. For example, the well-known default mode network (DMN) includes brain regions consistently found to be deactivated during effortful cognitive task execution (Buckner et al., 2008; Fox et al., 2005; Raichle et al., 2001). Interestingly, some of the classic DMN nodes, such as PCC, PCun, ACC, and medial PFC, were also found in our HR-fMRI analysis. This finding is in keeping with a number of studies linking activity in the DMN network to autonomic regulation. For instance, (Nagai et al., 2004) found a negative correlation between neural activity in vmPFC and OFC and tonic changes in skin conductance level (SCL), which were used to assess basal sympathetic tone. Moreover, increases in HR evoked during a handgrip task correlated with vmPFC deactivation in healthy individuals (Wong et al., 2007). Finally, a study investigating the relationship between cortical BOLD signal and beat-to-beat interval fluctuations at rest found a positive correlation between RR interval length, estimated by interpolating the RR time series, and vmPFC activity (Ziegler et al., 2009), which is consistent with our findings. Indeed, the CAN is likely not a static network operating independently from other canonical networks, but rather a collection of brain regions and structures that mediate autonomic outflow while also simultaneously playing other roles in the processing of specific tasks/stimuli/conditions. Therefore, distinct CAN components will be differentially engaged by various experimental manipulations and conditions, including the resting state. Interestingly, grey matter brainstem nuclei known to be involved in relaying brain signals to the ANS did not show statistically significant effects. This is probably due to technical limitations in imaging very

small structures in a problematic area to image as the brainstem, which could be partially overcome by further investigations at ultra-high-field (7T) (Chang et al., 2016).

There are some limitations of the present study that should be discussed. We estimated peripheral autonomic outflow from pulse signals for a joint HRV-fMRI analysis. Other autonomic series rather than heartbeat dynamics, including respiratory dynamics, could be investigated to more comprehensively uncover neural correlates of sympatho-vagal dynamics. Still, while the question of how to interpret, in neurobiological terms, the associations between fMRI measures and autonomic measures (here, HRV) remains open in any study using the BOLD signal as proxy measure of neuronal functioning, the HF measure is a marker of cardiac parasympathetic activity while HR is the result of a nonlinear, complex interaction between parasympathetic and ortosympathetic regulation of heart rate (Acharya et al., 2007). We therefore believe that the HF-HRV index represents a more specific source of autonomic control than the HR measure

However, variations in beat-to-beat time intervals can still be used as a general measure for heart-brain interactions (Ziegler et al., 2009), and are potentially useful in evaluating the central mechanisms of autonomic dysfunction in a broad group of pathological conditions. We chose to employ the preprocessed data made available via the HCP consortium which, amongst other state-of-the art procedures, has been denoised with the ICA-FIX strategy which was especially optimized for HCP data (Salimi-Khorshidi et al., 2014) to remove noise sources including physiological noise. Since it is not known how much physiological variance in the BOLD signal is removed by this method, it is possible that some residual physiological noise contamination is present in our results. However, given that we are investigating the effect of regressors of interest obtained from the plethysmography signal, we felt that it was best to not represent physiological noise by deriving regressors of no interest (e.g. RETROICOR, RVCOR (Chang and Glover, 2009)) from the same signal. We therefore opted for an unbiased and data-driven strategy. Our data-driven approach to data analysis, which was not prompted by a strong a priori hypotheses or a priori defined regions of interest, may result in a possible limitation with regards to specificity, i.e. to elucidating the precise roles that the brain structures we identified play in relation to the CAN. Future (e.g.) seed-based and hypothesis-driven studies are need to address these aspects in a targeted manner. Finally, we employed a canonical hemodynamic response function as a convolution kernel for both HF-HRV and HR. Although this is a reasonable assumption, future work should focus on the estimation of regionally specific transfer functions between HRV indices and BOLD signal.

In conclusion, we found that the CAN activity at rest (and in particular its cardiovagal modulation) includes a much wider network of brain regions than previously thought. This is possibly dependent on differences in CAN function during resting relative to task-related experimental conditions. Our results about CAN activity can serve as a stepping stone for future studies of the functional neuroanatomical correlates of the CAN in clinical populations in which task-based fMRI is unpractical or difficult to obtain.

ACCEPTED MANUSCRIPT

Acknowledgements

This work was supported by the US National Institutes for Health (NIH), Office of the Director (OT2-OD023867 to VN); National Center for Complementary and Integrative Health (NCCIH), NIH (P01-AT009965, R61-AT009306, R33-AT009306, R01-AT007550 to VN); the National Institute for Arthritis and Musculoskeletal and Skin Diseases (NIAMS), NIH (R01-AR064367 to VN); the Medical Research Council (MRC), UK (MR/P01271X/1 to LP); the American Heart Association (16GRNT26420084 to RB).

Declarations of interest: none

ACCEPTED MANUSCRIPT

References

Acharya, U.R., Joseph, K.P., Kannathal, N., Min, L.C., Suri, J.S., 2007. Heart rate variability. Advances in cardiac signal processing. Springer, pp. 121-165.

Allen, B., Jennings, J.R., Gianaros, P.J., Thayer, J.F., Manuck, S.B., 2015. Resting high-frequency heart rate variability is related to resting brain perfusion. Psychophysiology 52, 277-287.

Barbieri, R., Matten, E.C., Alabi, A.A., Brown, E.N., 2005. A point-process model of human heartbeat intervals: new definitions of heart rate and heart rate variability. Am J Physiol Heart Circ Physiol 288, H424-435.

Beissner, F., Meissner, K., Bar, K.J., Napadow, V., 2013. The autonomic brain: an activation likelihood estimation meta-analysis for central processing of autonomic function. J Neurosci 33, 10503-10511.

Benarroch, E.E., 1993. The central autonomic network: functional organization, dysfunction, and perspective. Mayo Clin Proc 68, 988-1001.

Benarroch, E.E., 2012. Central autonomic control. Primer on the Autonomic Nervous System (Third Edition). Elsevier, pp. 9-12.

Buckner, R.L., Andrews-Hanna, J.R., Schacter, D.L., 2008. The brain's default network: anatomy, function, and relevance to disease. Ann N Y Acad Sci 1124, 1-38.

Bush, G., Luu, P., Posner, M.I., 2000. Cognitive and emotional influences in anterior cingulate cortex. Trends Cogn Sci 4, 215-222.

Cechetto, D.F., Saper, C.B., 1990. Role of the cerebral cortex in autonomic function. In: Loewy, A.D., Spyer, K.M. (Eds.), Central Regulation of Autonomic Function. Oxford University Press, Oxford, pp. 208-223.

Chang, C., Glover, G.H., 2009. Effects of model-based physiological noise correction on default mode network anti-correlations and correlations. Neuroimage 47, 1448-1459.

Chang C, Metzger CD, Glover GH, Duyn JH, Heinze HJ, Walter M. Association between heart rate variability and fluctuations in resting-state functional connectivity. Neuroimage. 2013 Mar;68:93-104.

Chang, C., Raven, E.P., Duyn, J.H., 2016. Brain-heart interactions: challenges and opportunities with functional magnetic resonance imaging at ultra-high field. Philos Trans A Math Phys Eng Sci 374.

Colivicchi, F., Bassi, A., Santini, M., Caltagirone, C., 2004. Cardiac autonomic derangement and arrhythmias in right-sided stroke with insular involvement. Stroke 35, 2094-2098.

Critchley, H.D., 2005. Neural mechanisms of autonomic, affective, and cognitive integration. J Comp Neurol 493, 154-166.

Critchley, H.D., Mathias, C.J., Josephs, O., O'Doherty, J., Zanini, S., Dewar, B.K., Cipolotti, L., Shallice, T., Dolan, R.J., 2003. Human cingulate cortex and autonomic control: converging neuroimaging and clinical evidence. Brain 126, 2139-2152.

Critchley, H.D., Nagai, Y., Gray, M.A., Mathias, C.J., 2011. Dissecting axes of autonomic control in humans: Insights from neuroimaging. Auton Neurosci 161, 34-42.

de Morree, H.M., Rutten, G.J., Szabo, B.M., Sitskoorn, M.M., Kop, W.J., 2016. Effects of Insula Resection on Autonomic Nervous System Activity. J Neurosurg Anesthesiol 28, 153-158.

Devinsky, O., Morrell, M.J., Vogt, B.A., 1995. Contributions of anterior cingulate cortex to behaviour. Brain 118 (Pt 1), 279-306.

Duggento, A., Bianciardi, M., Passamonti, L., Wald, L.L., Guerrisi, M., Barbieri, R., Toschi, N., 2016. Globally conditioned Granger causality in brain-brain and brain-heart interactions: a combined heart rate variability/ultra-high-field (7 T) functional magnetic resonance imaging study. Philos Trans A Math Phys Eng Sci 374.

Etkin, A., Egner, T., Kalisch, R., 2011. Emotional processing in anterior cingulate and medial prefrontal cortex. Trends Cogn Sci 15, 85-93.

Farrell, M.J., Laird, A.R., Egan, G.F., 2005. Brain activity associated with painfully hot stimuli applied to the upper limb: a meta-analysis. Hum Brain Mapp 25, 129-139.

Fox, M.D., Snyder, A.Z., Vincent, J.L., Corbetta, M., Van Essen, D.C., Raichle, M.E., 2005. The human brain is intrinsically organized into dynamic, anticorrelated functional networks. Proceedings of the National Academy of Sciences of the United States of America 102, 9673-9678.

Gianaros, P.J., Van Der Veen, F.M., Jennings, J.R., 2004. Regional cerebral blood flow correlates with heart period and high-frequency heart period variability during working-memory tasks: Implications for the cortical and subcortical regulation of cardiac autonomic activity. Psychophysiology 41, 521-530.

Glasser, M.F., Sotiropoulos, S.N., Wilson, J.A., Coalson, T.S., Fischl, B., Andersson, J.L., Xu, J., Jbabdi, S., Webster, M., Polimeni, J.R., Van Essen, D.C., Jenkinson, M., Consortium, W.U.-M.H., 2013. The minimal preprocessing pipelines for the Human Connectome Project. Neuroimage 80, 105-124.

Goswami, R., Frances, M.F., Shoemaker, J.K., 2011. Representation of somatosensory inputs within the cortical autonomic network. Neuroimage 54, 1211-1220.

Griffanti, L., Salimi-Khorshidi, G., Beckmann, C.F., Auerbach, E.J., Douaud, G., Sexton, C.E., Zsoldos, E., Ebmeier, K.P., Filippini, N., Mackay, C.E., Moeller, S., Xu, J., Yacoub, E., Baselli, G., Ugurbil, K., Miller, K.L., Smith, S.M., 2014. ICA-based artefact removal and accelerated fMRI acquisition for improved resting state network imaging. Neuroimage 95, 232-247.

Kamath, M.V., Fallen, E.L., 1993. Power spectral analysis of heart rate variability: a noninvasive signature of cardiac autonomic function. Crit Rev Biomed Eng 21, 245-311.

Kober, H., Barrett, L.F., Joseph, J., Bliss-Moreau, E., Lindquist, K., Wager, T.D., 2008. Functional grouping and cortical–subcortical interactions in emotion: a meta-analysis of neuroimaging studies. Neuroimage 42, 998-1031.

Kurth, F., Zilles, K., Fox, P.T., Laird, A.R., Eickhoff, S.B., 2010. A link between the systems: functional differentiation and integration within the human insula revealed by meta-analysis. Brain Struct Funct 214, 519-534.

LeDoux, J., 2007. The amygdala. Curr Biol 17, R868-874.

LeDoux, J.E., 1992. Emotion and the amygdala.

Lombardi, F., Malliani, A., Pagani, M., Cerutti, S., 1996. Heart rate variability and its sympatho-vagal modulation. Cardiovasc Res 32, 208-216.

Luu, P., Posner, M.I., 2003. Anterior cingulate cortex regulation of sympathetic activity. Oxford University Press.

Malik, M., Bigger, J., Camm, A., Kleiger, R., Malliani, A., Moss, A., Schwartz, P., 1996. Heart rate variability. Standards of measurement, physiological interpretation, and clinical use. Task Force of the European Society of Cardiology and the North American Society of Pacing and Electrophysiology. Eur Heart J 17, 354-381.

Matsunaga, M., Isowa, T., Kimura, K., Miyakoshi, M., Kanayama, N., Murakami, H., Fukuyama, S., Shinoda, J., Yamada, J., Konagaya, T., Kaneko, H., Ohira, H., 2009. Associations among positive mood, brain, and cardiovascular activities in an affectively positive situation. Brain research 1263, 93-103.

McNab, J.A., Edlow, B.L., Witzel, T., Huang, S.Y., Bhat, H., Heberlein, K., Feiweier, T., Liu, K., Keil, B., Cohen-Adad, J., Tisdall, M.D., Folkerth, R.D., Kinney, H.C., Wald, L.L., 2013. The Human Connectome Project and beyond: initial applications of 300 mT/m gradients. Neuroimage 80, 234-245.

Mechias, M.L., Etkin, A., Kalisch, R., 2010. A meta-analysis of instructed fear studies: implications for conscious appraisal of threat. Neuroimage 49, 1760-1768.

Medford, N., Critchley, H.D., 2010. Conjoint activity of anterior insular and anterior cingulate cortex: awareness and response. Brain Struct Funct 214, 535-549.

Mesulam, M.M., Mufson, E.J., 1982. Insula of the old world monkey. I. Architectonics in the insulo-orbito-temporal component of the paralimbic brain. J Comp Neurol 212, 1-22.

Nagai, Y., Critchley, H.D., Featherstone, E., Trimble, M.R., Dolan, R.J., 2004. Activity in ventromedial prefrontal cortex covaries with sympathetic skin conductance level: a physiological account of a “default mode” of brain function. Neuroimage 22, 243-251.

Napadow, V., Dhond, R., Conti, G., Makris, N., Brown, E.N., Barbieri, R., 2008. Brain correlates of autonomic modulation: combining heart rate variability with fMRI. Neuroimage 42, 169-177.

Nee, D.E., Wager, T.D., Jonides, J., 2007. Interference resolution: insights from a meta-analysis of neuroimaging tasks. Cogn Affect Behav Neurosci 7, 1-17.

Nikolaou F, Orphanidou C, Papakyriakou P, Murphy K, Wise RG, Mitsis GD. Spontaneous physiological variability modulates dynamic functional connectivity in resting-state functional magnetic resonance imaging. Philos Trans A Math Phys Eng Sci. 2016 May 13;374(2067).

Nugent, A.C., Bain, E.E., Thayer, J.F., Sollers, J.J., 3rd, Drevets, W.C., 2011. Heart rate variability during motor and cognitive tasks in females with major depressive disorder. Psychiatry Res 191, 1-8.

Oppenheimer, S., Cechetto, D., 2016. The Insular Cortex and the Regulation of Cardiac Function. Compr Physiol 6, 1081-1133.

Raichle, M.E., MacLeod, A.M., Snyder, A.Z., Powers, W.J., Gusnard, D.A., Shulman, G.L., 2001. A default mode of brain function. Proc Natl Acad Sci U S A 98, 676-682.

Reyes del Paso, G.A., Langewitz, W., Mulder, L.J., van Roon, A., Duschek, S., 2013. The utility of low frequency heart rate variability as an index of sympathetic cardiac tone: a review with emphasis on a reanalysis of previous studies. Psychophysiology 50, 477-487.

Rubio, A., Van Oudenhove, L., Pellissier, S., Ly, H.G., Dupont, P., de Micheaux, H.L., Tack, J., Dantzer, C., Delon-Martin, C., Bonaz, B., 2015. Uncertainty in anticipation of uncomfortable rectal distension is modulated by the autonomic nervous system—a fMRI study in healthy volunteers. Neuroimage 107, 10-22.

Salimi-Khorshidi, G., Douaud, G., Beckmann, C.F., Glasser, M.F., Griffanti, L., Smith, S.M., 2014. Automatic denoising of functional MRI data: combining independent component analysis and hierarchical fusion of classifiers. Neuroimage 90, 449-468.

Saper, C.B., 2002. The central autonomic nervous system: conscious visceral perception and autonomic pattern generation. Annu Rev Neurosci 25, 433-469.

Sclocco, R., Beissner, F., Desbordes, G., Polimeni, J.R., Wald, L.L., Kettner, N.W., Kim, J., Garcia, R.G., Renvall, V., Bianchi, A.M., Cerutti, S., Napadow, V., Barbieri, R., 2016a. Neuroimaging brainstem circuitry supporting cardiovagal response to pain: a combined heart rate variability/ultrahigh-field (7 T) functional magnetic resonance imaging study. Philos Trans A Math Phys Eng Sci 374.

Sclocco, R., Kim, J., Garcia, R.G., Sheehan, J.D., Beissner, F., Bianchi, A.M., Cerutti, S., Kuo, B., Barbieri, R., Napadow, V., 2016b. Brain Circuitry Supporting Multi-Organ Autonomic Outflow in Response to Nausea. Cereb Cortex 26, 485-497.

Shackman, A.J., Salomons, T.V., Slagter, H.A., Fox, A.S., Winter, J.J., Davidson, R.J., 2011. The integration of negative affect, pain and cognitive control in the cingulate cortex. Nat Rev Neurosci 12, 154-167.

Smith, S.M., Vidaurre, D., Beckmann, C.F., Glasser, M.F., Jenkinson, M., Miller, K.L., Nichols, T.E., Robinson, E.C., Salimi-Khorshidi, G., Woolrich, M.W., Barch, D.M., Ugurbil, K., Van Essen, D.C., 2013. Functional connectomics from resting-state fMRI. Trends Cogn Sci 17, 666-682.

Sporns, O., 2014. Contributions and challenges for network models in cognitive neuroscience. Nat Neurosci 17, 652-660.

Thayer, J.F., Ahs, F., Fredrikson, M., Sollers, J.J., 3rd, Wager, T.D., 2012. A meta-analysis of heart rate variability and neuroimaging studies: implications for heart rate variability as a marker of stress and health. Neurosci Biobehav Rev 36, 747-756.

Thayer, J.F., Lane, R.D., 2007. The role of vagal function in the risk for cardiovascular disease and mortality. Biol Psychol 74, 224-242.

ACCEPTED MANUSCRIPT

Valenza, L. Citi, E.P. Scilingo, R. Barbieri, 2013. Point-Process Nonlinear Models with Laguerre and Volterra Expansions: Instantaneous Assessment of Heartbeat Dynamics, IEEE Transactions on Signal Processing, vol. 61, num. 11, pp. 2914-2926.

Valenza, G, L. Citi, E.P. Scilingo, and R. Barbieri. Inhomogeneous Point-process Entropy: an Instantaneous Measure of Complexity in Discrete Systems, Physical Review E, vol. 89 num. 5, 052803, 2014.

Valenza, G, L Citi, JP Saul, R Barbieri, 2018. Measures of Sympathetic and Parasympathetic Autonomic Outflow from Heartbeat Dynamics, Journal of Applied Physiology, vol. 125, num 1, pp. 19-39.

Valenza, G., Duggento, A., Passamonti, L., Diciotti, S., Tessa, C., Barbieri, R., Toschi, N., 2017. Resting-state brain correlates of instantaneous autonomic outflow. Conf Proc IEEE Eng Med Biol Soc 2017, 3325-3328.

Verberne, A.J., Owens, N.C., 1998. Cortical modulation of the cardiovascular system. Prog Neurobiol 54, 149-168.

Vogt, B.A., Finch, D.M., Olson, C.R., 1992. Functional heterogeneity in cingulate cortex: the anterior executive and posterior evaluative regions. Cereb Cortex 2, 435-443.

Wei, L., Chen, H., Wu, G.R., 2018. Heart rate variability associated with grey matter volumes in striatal and limbic structures of the central autonomic network. Brain Res 1681, 14-20.

Wong, S.W., Kimmerly, D.S., Masse, N., Menon, R.S., Cechetto, D.F., Shoemaker, J.K., 2007. Sex differences in forebrain and cardiovagal responses at the onset of isometric handgrip exercise: a retrospective fMRI study. Journal of applied physiology 103, 1402-1411.

Ziegler, G., Dahnke, R., Yeragani, V.K., Bar, K.J., 2009. The relation of ventromedial prefrontal cortex activity and heart rate fluctuations at rest. Eur J Neurosci 30, 2205-2210.

ACCEPTED MANUSCRIPT